Chapter 1 : Introduction

1.1 Motivation

In today's rapidly advancing world, the escalating demand for energy and the pursuit of more efficient resource utilisation are pivotal to fostering both economic growth and advancement of humanity. One of the most noteworthy advancements in recent years has been the development of multifunctional luminescent materials, with significant exploration into their potential applications across a variety of emerging fields. Lanthanide-activated phosphor materials, in particular, have attracted significant attention due to their outstanding technological performance and wide-ranging commercial applications. These materials find applications across a broad spectrum of fields, including display technologies, phosphor lamps, lasers, biomedical sensors, anti-counterfeiting systems, and optical amplifiers.

The first chapter of this thesis offers an in-depth exploration of the historical aspect and theoretical principles behind Lanthanides (Ln^{3+}) emissions. It also delves into key concepts such as host material dependence, the mechanisms underlying energy transfer processes, and the distinctive behaviours exhibited by inorganic host, complex and hybrid materials incorporating lanthanides. Finally, the study places particular emphasis on luminescent materials that exhibit temperature-dependent properties, exploring both their theoretical foundations and innovative methods for utilizing phosphor materials in temperature sensing applications. The chapter concludes by delineating primary objectives of the thesis, setting the stage for a deeper dive into the innovative potential of these materials.

1.2 Brief History of Luminescence

The fascination with luminescence has intrigued humanity since ancient times, as evidenced in ancient texts such as the Vedic scriptures of India and classical Chinese poetry, where the phenomena of glowing light from fireflies and glowworms were often employed as metaphors. Naturally occurring luminescence can be observed in various phenomena, including the light emission from glow-worms, the aurora borealis, fireflies, luminescent wood, sea algae, certain minerals, and microorganisms [1]. Aristotle (384–322 B.C.) and other contemporary Greek philosophers were among the earliest to observe and document the light emitted by bacteria and fungi [2][3]. The word "luminescence," derived from the Latin *lumen* meaning *light*, was first coined by Eilhard Wiedemann in 1888 to describe light emission processes not exclusively associated with heat [4]. Later, Vavilov refined this understanding by suggesting that luminescence can persist beyond the period of excitation. The study of photoluminescence underwent a notable progression during the 17th and 18th centuries, as people, motivated primarily by intellectual curiosity, began to explore the luminescent properties of inorganic materials. These materials, later known as "phosphors," were found to emit light when exposed to various forms of energy, including heat, light, or electrical fields [5]. In the early 1600s, Italian alchemist Vincenzo Cascariolo made the first documented discovery of an artificial phosphor while attempting to extract gold from barite mineral ($BaSO_4$) [6]. Instead, he found that barium sulfide (BaS) emitted a glow after being exposed to sunlight, though the phenomenon was not scientifically understood at the time.

The systematic study of luminescence, however, began in earnest with the advent of spectroscopy, which significantly advanced our understanding of the fundamental laws governing absorption and emission phenomena. In 1852, George Stokes established an

empirical law stating that the wavelengths of emitted luminescence are longer than those of the incident radiation. Early observations about luminescence, rooted in a profound curiosity about nature's mysteries, laid the groundwork for later exploration, yet systematic scientific study of luminescence did not commence until the mid-19th century. By the end of the century, scientific understanding of the luminescence process had advanced significantly, leading to the classification of various types of luminescence. These categories were defined based on the distinct processes through which energy is converted into light, including bioluminescence, thermoluminescence, electroluminescence, photoluminescence, radioluminescence, chemiluminescence, among others [7].

1.3 Scientific Advances and the Role of Phosphors

Phosphor materials, characterized by their ability to emit light upon external stimulation, became a central focus of scientific investigation in the late nineteenth and early twentieth centuries. During this pivotal period, researchers were fascinated by the remarkable ability of these materials to convert energy into visible light. This property not only deepened theoretical understanding of luminescence but also sparked major breakthroughs across several technological domains. Wiedemann and Schmidt (1895) documented the thermoluminescence of materials such as fluorite [manganese-doped calcium fluoride (CaF_2: Mn), providing early examples of how impurities in a crystal could influence its luminescent properties[8]. A notable example of phosphors includes BaS:Cu^+ (which exhibits orange and red emissions), ZnS:Cu^+,Co^{2+} (characterized by green emission), as well as CaS, SrS, and ($Ca_{1-x}Sr_x$)S:Bi^{3+}, Eu^{2+}, or Ce^{3+}, collectively referred to as Lenard's phosphors (1928), which have played a significant role in the historical development of luminescent materials. Table 1.1 presents a chronological overview of key discoveries in luminescence, highlighting the

type of discovery, excitation source, luminescent materials used, and their emission colours. It spans from the early 1600s to the 1970s, showcasing the evolution of luminescent technologies such as gas-discharge lamps, cathode-ray tubes, and the development of fluorescent and laser materials.

Table 1.1 Early milestones in the discovery of luminescent materials and devices.

Year	Kind of Discovery	Excitation Source	Various Luminescent Material	Emission Color
~1600	Stone of Bologna	sunlight	$BaSO_4$ (BaS)	yellow
1858	Geißler's tube	gas-discharge (Hg)	UV	-
1859	Becquerel	gas-discharge (Hg)	ZnS	yellow-white
1895	X-rays (by Röntgen)	X-ray	none (photographic plate)	-
1896	X-ray intensifier (by Pupin)	X-ray	$CaWO_4$	blue
1896	Fluorescent lamp (by Edison)	gas-discharge (Hg)	$CaWO_4$	blue
1897	Braun's tube	cathode-ray	$CaWO_4$	blue
1916	Neon discharge lamp (by Claude)	gas-discharge (Ne)	none	red
1925	Black-and-white television	cathode-ray	$ZnS:Ag^+$; $(Zn,Cd)S:Ag^+$	blue; yellow
1937	Neon discharge lamp (by Claude)	gas-discharge (Ne)	$CaWO_4$; $Zn_2SiO_4:Mn^{2+}$	blue; green
1938	Fluorescent lamp	gas-discharge (Hg)	$MgWO_4$; $(Zn,Be)_2SiO_4:Mn^{2+}$	blue-green; green-red
1941	Radar screen	cathode-ray	$(Zn,Cd)S:Cu^+,Al^{3+}$	green
1946	Insect lamps	gas-discharge (Hg)	$CaWO_4$	blue
1960	Color television	cathode-ray	$ZnS:Ag^+$; $(Zn,Cd)S:Cu^+,Al^{3+}$; $(Zn,Cd)S:Ag^+$	blue; green; red
1960	Laser (by Maiman)	-	$Al_2O_3:Cr^{3+}$	red
1972	Computed tomography (by Houndsfield)	X-ray	$NaI:Tl^+$	green
1972	Rare-earth phosphors	gas-discharge (Hg)	$Sr_3(PO_4)_5Cl:Eu^{3+}$; $LaPO_4:Ce^{3+},Tb^{3+}$; $Y_2O_3:Eu^{3+}$	blue; green; red

Regarding the lanthanide luminescence, in 1885, Welsbach's discovery of the incandescent properties of rare earth elements (REs) laid the foundation for the development of efficient commercial gas mantles[3]. In 1907, Becquerel conducted the first spectroscopic

study of rare-earth salts at low temperatures, noting that the broad absorption bands were resolved into distinct sharp spectral lines. This observation was later substantiated by Van Vleck in 1937, who proposed that these absorptions originated from intra-4f n electronic transitions in lanthanides. In 1942, it was found that complexes of europium, terbium, and samarium exhibited peculiar luminescence characteristics when stimulated by ultraviolet radiation. However, a major advancement in phosphor technology came in 1964 with the development of YVO_4:Eu phosphors, a highly efficient red-emitting cathodoluminescent phosphor used in colour television[9]. Dieke (1967) provided a pioneering compilation of the absorption spectra and energy levels of rare-earth ions in their triply ionized state. In addition. the concept of upconversion in Ln^{3+} ions was initially proposed by Bloembergen in 1959, but it was realized experimentally by Auzel in 1966, following the advent of laser technology. This discovery marked the beginning of a systematic investigation of photoluminescent materials and their application in different domain of scientific as well as commercial field or general field. Our focus is specifically on exploring the photoluminescence properties of various materials. These discoveries marked the onset of a systematic exploration of photoluminescent materials, thereby facilitating their widespread application across various scientific disciplines, commercial sectors, and broader domains of use.

Modern phosphors are pivotal in numerous advanced applications, significantly enhancing technologies across lighting, sensing, biomedical, and energy fields. Their adaptability through doping with rare earth (RE) and transition metal (TM) ions ensures emission customization, allowing their applications to span a wide range of technological domains. Below, a detailed discussion highlights their critical roles across diverse fields.

Lighting Applications: Phosphors are essential components of white light-emitting diodes (WLEDs), offering high energy efficiency, improved color rendering, and reduced environmental impact compared to conventional lighting systems. Down-shifting (DS) luminescent materials, which convert high-energy photons into lower-energy emissions, dominate lighting applications. They exhibit high quantum efficiency, low thermal quenching, and broad emission bands, making them ideal for commercial and industrial lighting. Moreover, advancements in RE-doped phosphors have enabled the tuning of light quality, critical for creating warm or cool lighting environments tailored to specific needs, such as healthcare, horticulture, and retail.

Temperature Sensing and Optical Thermometry: Luminescent phosphors provide a contactless and non-invasive method for precise temperature measurements. By utilizing fluorescence intensity ratio (FIR) techniques based on thermally coupled energy levels of RE ions such as Er^{3+}, Tm^{3+}, and Ho^{3+}, these materials can measure temperatures with high sensitivity and reliability. Non-thermally coupled levels (NTCLs) provide an alternative mechanism for sensors, enabling their use in extreme conditions, such as microfluidics, marine research, and food storage. For instance, phosphors such as Yb^{3+}/Er^{3+} and Yb^{3+}/Ho^{3+} doped materials exhibit well-defined emission changes with temperature, enabling their use in biomedicine to monitor cellular environments or detect tumors and inflammations.

Biomedical Applications: Phosphors, particularly up-conversion nanophosphors (UCNPs), have transformed biomedical imaging and drug delivery. UCNPs convert low-energy near-infrared (NIR) photons into visible or ultraviolet emissions, offering advantages like deep tissue penetration, minimal photodamage, and reduced autofluorescence. These properties are critical for advanced bioimaging and diagnostics, where UCNPs enable real-time

visualization of biological processes and targeted drug delivery systems. Functionalized phosphors coated with biocompatible materials such as silica or polymers enhance their compatibility with living tissues. For example, phosphors doped with Er^{3+}, Tm^{3+}, and Yb^{3+} have been used to deliver anti-cancer drugs directly to tumor cells, ensuring high precision and reduced side effects. Additionally, their integration into multi-modal imaging techniques, such as combining NIR bioimaging with MRI or CT, has improved diagnostic accuracy.

Anti-Counterfeiting and Security: Luminescent materials also find applications in anti-counterfeiting and secure documentation. Phosphors doped with RE or TM ions offer unique spectral signatures that can be incorporated into products, documents, or currency to prevent forgery. These materials are activated under specific wavelengths, emitting distinct colors or patterns visible under ultraviolet or NIR excitation. Their use in security measures ensures high reliability and minimal replication risk.

Photovoltaics and Energy Applications: In solar energy, phosphors address the spectral mismatch challenge in photovoltaic cells. Down-conversion and up-conversion phosphors are used to modify the solar spectrum, allowing better utilization of NIR radiation. For instance, phosphors like Yb^{3+}/Er^{3+} doped materials are incorporated into solar cell designs to capture NIR light and emit visible light, which can be efficiently absorbed by the photovoltaic material. These advancements enhance energy conversion efficiency, reducing the reliance on traditional energy sources and supporting the transition to sustainable energy systems.

Future Directions and Challenges: Despite these advancements, challenges remain in optimizing phosphors for specific applications. Issues such as thermal quenching, cytotoxicity in biomedical applications, and limited quantum efficiency in certain hosts require continued research. Innovations in material synthesis, surface engineering, and the development of

hybrid systems combining RE and TM ions are paving the way for next-generation phosphors with superior performance.

In summary, phosphors have emerged as indispensable materials across various high-tech domains. Their ability to harness and manipulate light makes them critical for innovations in lighting, sensing, biomedical imaging, anti-counterfeiting, and energy. Ongoing research and technological integration continue to unlock new potentials, reinforcing their role in shaping future technologies.

1.4 Overview of Rare-earth elements

The lanthanide series, consisting of 15 chemical elements from lanthanum (La, atomic number 57) to lutetium (Lu, atomic number 71), is renowned for its exceptional optical, magnetic, and electronic properties. Table 1.2 provides details list of the rare-earth element's discovery in chronological order[10]. The discovery of lanthanides dates back to the late 18th and early 19th centuries. Cerium (Ce), the first lanthanide to be identified, was discovered in 1803 by Martin Heinrich Klaproth, Jöns Jakob Berzelius, and Wilhelm Hisinger. As the 19th century advanced, additional lanthanides were uncovered through the analysis of rare earth minerals. The understanding of these elements significantly advanced in the early 20th century with the development of more sophisticated analytical techniques, enabling scientists to isolate and characterize all lanthanides. This progress led to the revision of the periodic table to include the lanthanide series as f-block elements, acknowledging their distinctive role in the periodic system. Lanthanides became prominent after the discovery of ytterbite (later renamed gadolinite) by Lieutenant Karl Arrhenius in 1787 in Ytterby village, Sweden[11]. This discovery marked the beginning of a systematic study of these elements. Fig. 1.1 illustrates the periodic table, highlighting the series of lanthanide element.

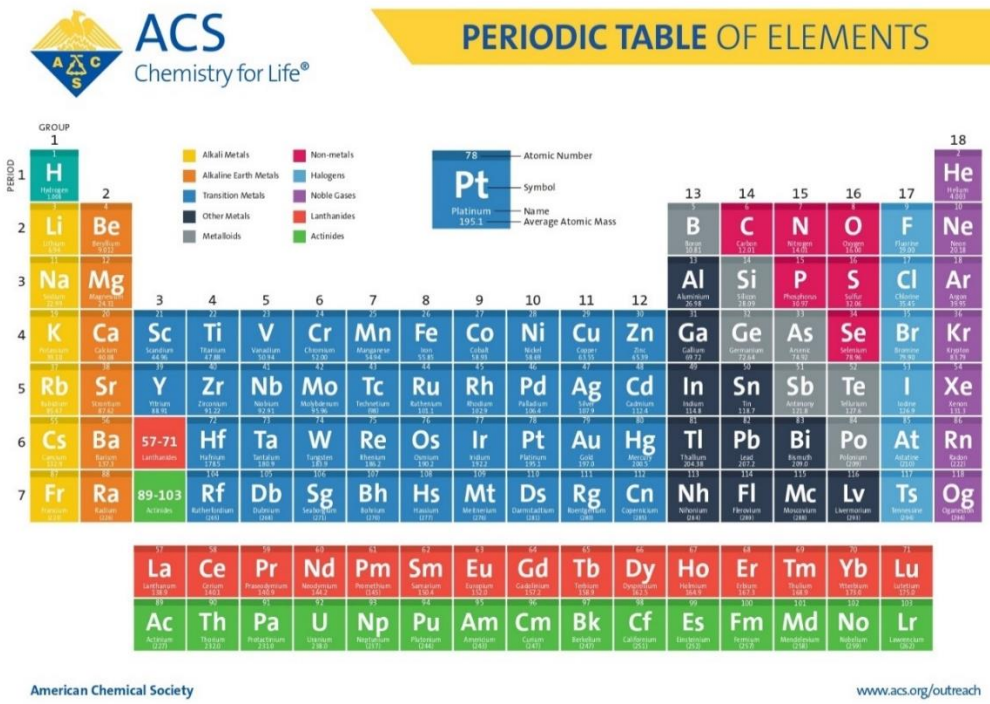

Figure 1.1 Periodic table of elements showing the position of lanthanides [https://www.acs.org/education/whatischemistry/periodictable.html.

Table 1.2 List of the rare-earth element's discovery in chronological order[10].

Elements and Atomic Numbers	**Symbol**	**Discoverer**	**Year**
Yttrium [39]	Y	Johan Gadolin, a Finnish chemist	1794
Cerium [58]	Ce	Jöns Jacob Berzelius and Wilhelm von Hisinger, Swedish chemist	1804
Lanthanum [57]	La	Carl Gustaf Mosander, a Swedish Chemist	1839
Terbium [65] and Erbium [68]	Tb & Er	Carl Gustaf Mosander, a Swedish Chemist	1843
Ytterbium [70]	Yb	Jean Charles Galissard de Marignac, a Swiss Chemist	1878
Samarium [62]	Sm	Paul-Emile Lecoq de Boisbaudran, a French chemist	1879
Scandium [21]	Sc	Lars Fredrik Nilson, a Swedish chemist	1879
Thulium [69] and Holmium [67]	Tm & Ho	Per Theodor Cleve, a Swedish chemist	1879
Gadolinium [64]	Gd	Jean Charles de Galissard, a Swiss Chemist	1880

Neodymium [60] and Praseodymium [59]	Nd & Pr	Carl F. Auer von Welsbach, German Chemist	1885
Dysprosium [66]	Dy	Paul- Emile Lecoq de Boisbaudran, a French Chemist	1886
Europium [63]	Eu	Eugene-Antole Demarcay, a French Chemist	1896

Lanthanides, together with scandium (Sc) and yttrium (Y), are often grouped under the term "rare earth elements" (REEs) because of their similar physical and chemical properties. Despite being relatively abundant in the Earth's crust, the term "rare earth" originated from the early challenges in isolating these elements [12]. Actually, the term ‘rare’ lanthanides are not particularly scarce. For example, Thulium (Tm), the least abundant lanthanide, is still more common than metals like Cadmium or Silver. Lighter lanthanides are generally more abundant in ores, which makes them easier to extract. Lanthanides are essential in numerous technological applications due to their unique electronic, optical, and magnetic properties, supporting energy-efficient lighting, lasers, data storage, catalysts, and renewable energy technologies. Their versatility makes them crucial across industries including, magnetic materials for data storage, catalysts, renewable energy technologies, lighting, lasers, medical imaging, and optoelectronics, underscoring their growing significance in both established and emerging fields.

1.4.1 Distinguished Characteristics of Lanthanides

Lanthanides share several common characteristics due to their similar electronic configurations. The lanthanide series, spanning atomic numbers 57 to 71 (from Lanthanum to Lutetium), features elements whose electron configurations are primarily characterized by the progressive filling of the 4f orbitals. All lanthanide elements have the general electron configuration $[Xe]4f^n5d^{0,1}6s^2$, where [Xe] represents the electron configuration of inert gas Xenon (54), and the valence electrons ($n = 1 - 14$) are added to the 4f, 5d, and 6s orbitals.

Whereas, the electronic configurations of Scandium (Sc) and Yttrium (Y) are [Ar] $3d^1$ $4s^2$ and [Kr] $4d^1$ $5s^2$, respectively, resulting in partially filled d-orbitals. Table 1.3 provides detailed information about the lanthanide series elements, including their atomic and ionic radii, electronic configurations, and ground-state term symbols. It highlights the trend of decreasing ionic radii and the variations in electronic configurations as each element progresses through the series.

As apparent from electronic configuration, the partially filled 4f orbitals of the lanthanides are effectively shielded by the outer $5s^2$ and $5p^6$ orbitals, which limit the influence of external factors, resulting in similar chemical behaviour and distinctive optical properties [13]. This shielding also results in minor crystal-field splitting, producing sharp electronic spectra compared to d-block metals [14]. One of the most distinctive features of lanthanides is the lanthanide due to increase in effective nuclear charge ($Z_{eff.}$). As the atomic number increases across the series, the atomic and ionic radii steadily decrease due to the increasing nuclear charge, which pulls electrons closer to the nucleus. This contraction profoundly affects lanthanides' bonding, coordination numbers, and reactivity [15]. As a result, lanthanides generally exhibit high coordination numbers (ranging from 6 to 12), and ligand steric factors rather than crystal-field effects primarily determine their coordination geometries. The partially filled 4f orbitals are responsible for the unique absorption and emission spectra of the lanthanide elements. The weak shielding leads to the splitting of energy levels due to the interactions between the 4f electrons and the crystal field in a complex environment, which is important in applications like phosphors, lasers, and other lanthanide-based materials. Lanthanides are characterised by their high electro-positivity and predominantly exist as +3 oxidation state ions. However, certain elements including Sm, Nd,

Eu, Dy, Tm, and Yb can also display a +2 state, whereas Ce, Pr, and Tb are known to exhibit +4 oxidation states, respectively [16]. The reactivity of lanthanides is generally higher than that of d-block metals, resembling the behaviour of group II elements[12]. Lanthanides form ionic complexes that undergo facile exchange of ligands, and they tend to bond with highly electronegative anionic ligands, such as oxygen and fluorine. Their high hydration energy leads to forming hydrated complexes, which can sometimes complicate the assignment of coordination numbers. Insoluble hydroxides tend to precipitate at neutral pH unless complexing agents are present, making lanthanide chemistry distinct from other metal ions in many ways [15].

Table 1.3 List of lanthanide ions, atomic number, radii, electronic configuration, and ground state[17].

Chemical Element	**Atomic Number (Z)**	**Atomic Radii (pm)**	**Ionic Radii of Ln^{3+} (pm)**	**Electronic configuration of Ln**	**Electronic configuration of Ln^{3+}**	**Ground State**
La	57	187.7	103.2	[Xe] $4f^0$ $5d^1$ $6s^2$	[Xe] $4f^0$	$^1S_0$
Ce	58	182.5	101.0	[Xe] $4f^2$ $5d^0$ $6s^2$	[Xe] $4f^1$	$^2F_{5/2}$
Pr	59	182.8	99.0	[Xe] $4f^3$ $5d^0$ $6s^2$	[Xe] $4f^2$	$^3H_4$
Nd	60	182.1	98.3	[Xe] $4f^4$ $5d^0$ $6s^2$	[Xe] $4f^3$	$^4I_{9/2}$
Pm	61	181.0	97.0	[Xe] $4f^5$ $5d^0$ $6s^2$	[Xe] $4f^4$	$^5I_4$
Sm	62	182.2	95.8	[Xe] $4f^6$ $5d^0$ $6s^2$	[Xe] $4f^5$	$^6H_{5/2}$
Eu	63	204.2	94.7	[Xe] $4f^7$ $5d^0$ $6s^2$	[Xe] $4f^6$	$^7F_0$
Gd	64	180.2	93.8	[Xe] $4f^8$ $5d^0$ $6s^2$	[Xe] $4f^7$	$^8S_{7/2}$
Tb	65	178.2	92.3	[Xe] $4f^9$ $5d^0$ $6s^2$	[Xe] $4f^8$	$^7F_6$
Dy	66	177.3	91.2	[Xe] $4f^{10}$ $5d^0$ $6s^2$	[Xe] $4f^9$	$^6H_{15/2}$
Ho	67	176.6	90.1	[Xe] $4f^{11}$ $5d^0$ $6s^2$	[Xe] $4f^{10}$	$^5I_8$
Er	68	175.7	89.0	[Xe] $4f^{12}$ $5d^0$ $6s^2$	[Xe] $4f^{11}$	$^4I_{15/2}$
Tm	69	174.6	88.0	[Xe] $4f^{13}$ $5d^0$ $6s^2$	[Xe] $4f^{12}$	$^3H_6$
Yb	70	194.0	86.8	[Xe] $4f^{14}$ $5d^0$ $6s^2$	[Xe] $4f^{13}$	$^2F_{7/2}$
Lu	71	173.4	86.1	[Xe] $4f^{14}$ $5d^1$ $6s^2$	[Xe] $4f^{14}$	$^1S_0$

1.4.2 Spectroscopy of Lanthanides

The optical properties of lanthanide ions are characterized by their unique electronic structure, particularly the partially filled 4f orbitals, which are effectively shielded by the outer 5s and 5p orbitals. This shielding leads to sharp, well-defined absorption and emission lines, in contrast to the broader spectra of transition metal-doped phosphors. These distinct spectral features were first observed by Becquerel in 1907 in rare-earth salts, sparking early theoretical investigations by Bethe (1930) and Kramer's (1930). Freed and Spedding (1929) further explored low-temperature absorption spectra, while Van Vleck (1937) addressed transitions that violated Laporte's rule. Emissions from lanthanides primarily result from 4f-4f and 4f-5d transitions, and their long fluorescence lifetimes, due to spin-forbidden transitions, make them well-suited for time-resolved fluorescence applications. The application of crystal-field theory allowed for more precise energy level assignments, with Dieke (1967) calculating the energy levels of trivalent ions.

The overarching theoretical framework for understanding rare-earth (RE) spectra involves solving the Hamiltonian, which includes interaction terms for free ion interactions, crystal field effects, electromagnetic fields, lattice vibrations, and ion-ion interactions.

$$H = H_{free\ ion} + V_{Site} + V_{EM} + V_{Vibrational} + V_{ion-ion} \quad \dots (1.1)$$

$H_{free\ ion}$: Hamiltonian of an isolated ion, comprising Coulombic, spin-orbit, and central field interactions, V_{Site} : Crystal field effects from the local environment, V_{EM}: Interaction with electromagnetic fields, $V_{Vibrational}$: Interaction with lattice vibrations (phonons), and $V_{ion-ion}$: Ion-ion interactions.

The free ion Hamiltonian is expanded into central field, residual Coulombic, and spin-orbit terms, with the Coulombic interactions splitting 4f electronic states and the spin-orbit coupling further dividing them into (J)-states, while crystal field splitting has a smaller impact. The $H_{free\ ion}$ term can be expanded as:

$$H_{free\ ion} = H_{cf} + H_{rc} + H_{so} \quad \ldots (1.2)$$

H_{cf} $(10^2 cm^{-1})$: Central field approximation, describing interactions between electrons and the nucleus, H_{rc} $(10^2 cm^{-1})$: Residual Coulombic interactions causing splitting of 4f electronic states, and H_{so} $(10^3 cm^{-1})$: Spin-orbit interaction, splitting energy levels into (J)-states. The residual Coulombic term H_{rc} splits the 4f electronic states into terms described by (L) and (S), while the spin-orbit H_{so} term further splits these terms into (J)-states. The shielding of 4f electrons by the 5s, 5p, and 6s orbitals causes only minor splitting of the $^{2S+1}L_J$ levels, with the extent of this splitting described by Crystal Field Theory through the inclusion of H_{cf} terms. This theory describes the interaction between the lanthanide ion and the electric field of the surrounding host lattice. The crystal-field potential at the ion site can be represented as a power series of tensor operators, as outlined by Wybourne (1965).

$$V_{site} = \sum_{iqk} B_q^k \left[C_q^k\right] i \quad \ldots (1.3)$$

where the summation over $\boldsymbol{i}$ involves all the 4f electrons of the ion. B_q^k is the radial-dependent part of the one-electron crystal-field interaction, representing the expansion coefficients known as *crystal-field parameters*. For f-electrons, $k \leq 6$. These parameters depend on the electron density and the host lattice structure and can be determined empirically from experimental data and $k \leq 6\ is$ many-electron spherical tensor operators corresponding to the $4f^n$ configuration.

The even k terms in the series split the free-ion J - multiples into *Stark components*, typically separated by 10–100 cm^{-1}. This splitting is governed by the triangle rule for the addition of angular momentum $I_1 + I_2 \leq k$, with the possible values of k and q being constrained by the ion's point symmetry. For example, under cubic symmetry, the splitting is minimal, while under lower symmetries, such as tetragonal or hexagonal, the J- multiplets split into a greater number of Stark components. Which means, the symmetry of the ion's environment can be inferred from the number of Stark components observed experimentally. The odd k terms in the crystal field Hamiltonian introduce a mixing of states with opposite parity into the 4f configuration. While these terms do not affect the positions of the energy levels, they significantly influence the strengths of optical transitions between levels, enabling otherwise forbidden transitions.

Lanthanide ions follow specific selection rules for electronic transitions, governed by odd-parity electric dipole (ED), even-parity magnetic dipole (MD), and electric quadrupole (EQ) operators. In centrosymmetric environments, the Laporte rule forbids transitions between states of the same parity, making 4f-4f transitions disallowed. However, in non-centrosymmetric environments, such as when lanthanide ions are doped in a host material, crystal field perturbations relax these parity restrictions, allowing partial 4f-4f transitions. These are referred to as induced or forced electric dipole transitions. Table 1.4 presents the selection rules for Electric Dipole, Magnetic Dipole, and Electric Quadrupole transitions, detailing the allowed changes in parity, spin (ΔS), orbital angular momentum (ΔL), and total angular momentum (ΔJ). These induced electric dipole transitions give rise to sharp spectral features across UV to NIR regions, although their oscillator strength is weak (10^{-6}). These transitions, crucial for luminescence in rare-earth-doped materials, are further influenced by

interactions with phonon states in the crystal lattice, causing shifts and splitting of energy levels. These effects underscore the intricate interplay between the lanthanide ions and their host matrix, which significantly influences the tuning of their optical properties.

Table 1.4 Selection rules for intra 4f-4f transitions for REs ions[18].

Operator	Parity	ΔS	ΔL	ΔJ*
Electric Dipole	Opposite	0	≤6	≤6 (2, 4, 6 if J or J' = 0)
Magnetic Dipole	Same	0	0	0, ±1
Electric Quadrupole	Same	0	0, ±1, ±2	0, ±1, ±2

*J = 0 ⟶ J' = 0 transition is always a forbidden transition.
J = 0 ⟶ J' = 1,3,5 transitions appear with weak intensity.
J = 0 ⟶ J' = 2,4,6 transitions appear with large intensity.

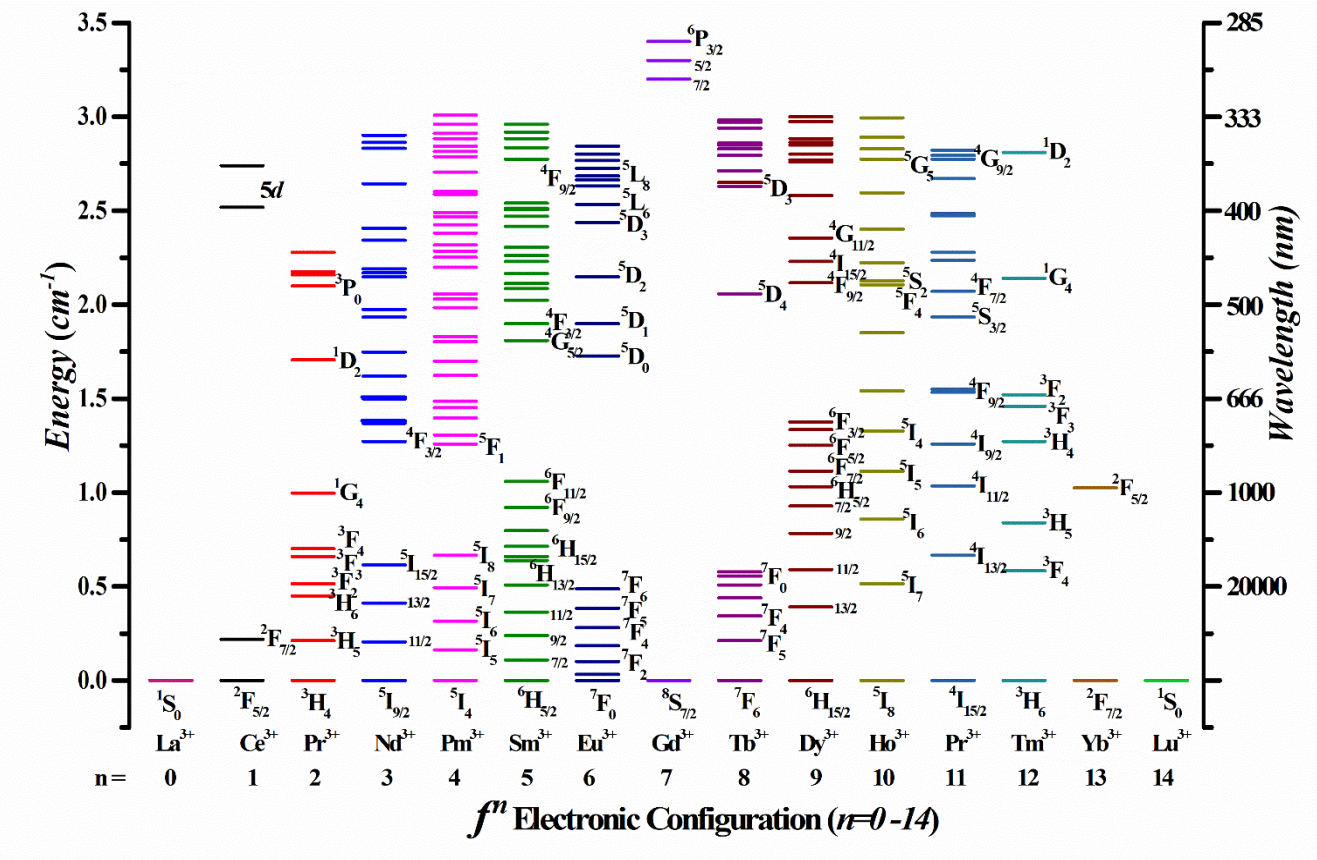

Figure 1.2 The list of possible splitting of lanthanides (Ln^{3+}) energy levels[19].

Lanthanides exhibit a diverse range of optical properties due to their unique electron configurations, although elements such as Lanthanum (La) and Lutetium (Lu) show minimal optical activity due to their 4f orbitals being either empty (La) or fully filled (Lu), leading to the absence of the sharp emission lines characteristic of lanthanides with partially filled 4f orbitals. Fig 1.2 illustrates the Dieke diagram, which maps the energy levels and transitions of trivalent lanthanide ions (e.g., Er^{3+}, Ho^{3+}, Tm^{3+}, Yb^{3+}), helping to identify excitation and emission pathways [19]. Among the optically active lanthanides, Ce^{3+} (Cerium) and Gd^{3+} (Gadolinium) are notable for their deep ultraviolet (UV) excitation and emission, acting as effective sensitizers by transferring energy through 4f-5d transitions to adjacent lanthanide or any optically active centres ions. Praseodymium (Pr^{3+}) produces both UV and yellow-orange emissions, while Thulium (Tm^{3+}) is notable for its emissions in the blue and near-infrared (NIR) regions (472 nm and 800 nm), as well as temperature-dependent bands near 650 nm and 700 nm. In addition, when it comes to achieving emissions in the green**,** yellow, and red regions, a variety of lanthanide ions are utilized, including Samarium (Sm^{3+})**,** Europium (Eu^{3+})**,** Terbium (Tb^{3+})**,** Dysprosium (Dy^{3+})**,** Holmium (Ho^{3+})**,** Thulium (Tm^{3+})**,** and Erbium (Er^{3+})**.** The specific emission colour depends on the selection of host material, additional foreign element doping and also optimizing the particular 4f-4f transitions within the lanthanide ion, making these elements highly suitable for color-tunablity and other application. Lanthanides like Neodymium (Nd^{3+}), Erbium (Er^{3+}), and Ytterbium (Yb^{3+}) are commonly used to generate near-infrared (NIR) emissions within the 700–2500 nm range. Among these, Ytterbium (Yb^{3+}) is particularly effective in up-conversion processes, where it facilitates the conversion of lower-energy infrared photons into higher-energy visible or ultraviolet light. The inherent up-conversion properties of lanthanides can be further enhanced

by incorporating Yb^{3+} ions, typically referred to as sensitizer ions, in conjunction with other activator ions, thereby enabling more efficient sensitization and improving up-conversion emission. A concise review of the conventional downconversion and distinctive upconversion phenomena is essential to elucidate the energy transfer mechanisms inherent in each process, thereby facilitating a more comprehensive understanding of the emission behaviour of lanthanide ions in specific host materials.

1.4.2.1 *Downconversion Phenomenon*

Downconversion (DC) is a linear Stokes-type process in which a material absorbs a high-energy photon, typically from UV or visible light, and subsequently re-emits the energy as lower-energy photons, often in the visible or near-infrared range. This phenomenon is of considerable interest in luminescent materials because of its diverse applications in technologies such as LEDs, solar cells, lasers, bioimaging, and optoelectronic devices. Through photon energy modulation through DC, materials can enhance performance and efficiency, enabling novel functionalities. DC can be classified into two types based on the underlying mechanisms and efficiency: (i) Downshifting (DS) and (ii) Quantum Cutting (QC).

1.4.2.1.(i) Downshifting Process

Downshifting refers to a single-photon downconversion process in which a high-energy photon is absorbed and subsequently re-emitted as a lower-energy photon. This conversion process is limited by an energy efficiency of 100% or less, as some energy is inevitably lost through non-radiative mechanisms. This phenomenon is commonly observed in fluorescent materials, including lanthanides and transition metal-activated compounds, which absorb UV light and emit in the visible or NIR regions. In certain cases, self-activated hosts can also

exhibit this property. The energy-level mechanism underlying downshifting is depicted in Fig 1.3, which illustrates the conversion pathway and the corresponding energy states [20]. It is commonly used in devices such as UV-absorbing coatings, solar cell enhancers, LEDs, and fluorescent lamps, where it boosts light efficiency and provides protection against harmful UV radiation.

1.4.2.1.(ii) Quantum Cutting Process

Quantum cutting (QC) is a process in which a single high-energy photon is converted into two or more lower-energy photons, enabling photon conversion efficiencies that can theoretically exceed 100%. This phenomenon holds significant promise for improving light-harvesting performance in solar cells and similar devices, as it enhances the capture and utilization of high-energy photons. The QC mechanism was first identified by Dexter in 1957, and later, Wegh *et al.* (1999) observed visible QC in the ion pair Gd^{3+}-Eu^{3+}. QC can occur through cascade emissions in single-doped systems or via energy transfer in co-doped phosphors. Notably, this cascade effect has been observed in phosphors doped with rare-earth ions such as Pr^{3+}, Tm^{3+}, and Gd^{3+}, which emit sequential photons after high-energy excitation. As depicted in Fig 1.3, the QC process involves energy-level transitions that lead to the emission of multiple photons per excitation, offering a highly efficient method for photon generation [21].

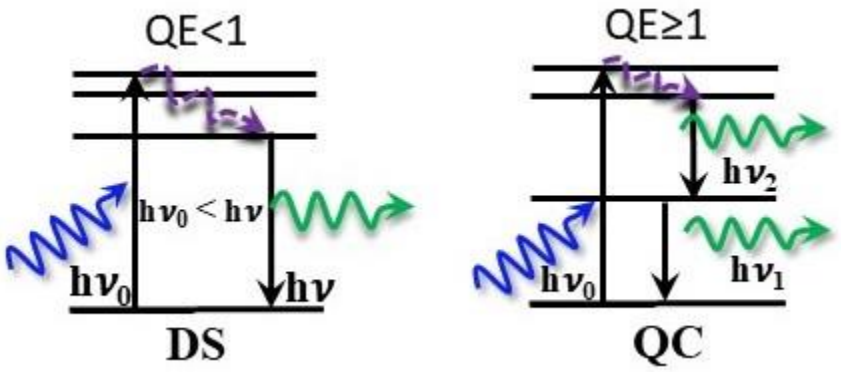

Figure 1.3 Schematic energy level diagram representing the downshifting and the Quantum Cutting process.

1.4.2.2 *Up-conversion Phenomenon*

The distinctive upconversion phenomenon is an anti-Stokes process in which low-energy photons, typically in the infrared (IR) or near-infrared (NIR) regions, are absorbed and converted into higher-energy photons, such as visible or ultraviolet (UV) light, through the sequential absorption of NIR photons via non-linear energy transfer mechanisms. Various multiphoton absorption phenomena occur in optical materials, where two or more low-energy photons combine to generate high-energy photons, such as Two-Photon Excited Fluorescence (TPEF), Second-Harmonic Generation (SHG), and Upconversion (UC). Among these, TPEF and SHG require high photon densities and also the formation of virtual energy states, which rely on on coherent or high-intensity pumping. UC occurs through the sequential absorption of low-energy photons, with electrons transitioning through real energy states before reaching higher-energy levels and emitting photons at shorter wavelengths than the excitation source. First mentioned by Auzel and Ovsyakin in 1966, UC does not demand high excitation intensities or coherent pumping, allowing it to be effective even at low excitation power, and the presence of metastable intermediate states that facilitate sequential photon absorption and energy transfer. Interesting to mention here, UC emission intensity is proportional to the n^{th} power of the NIR excitation intensity ($I \propto P^n$), where *n* represents the number of photons

absorbed to produce one high-energy photon. The UC process in lanthanide-doped materials, with their abundant energy levels, involves various energy transfer mechanisms shown in Fig 1.4, typically categorized as: (a) Ground/Excited State Absorption (GSA/ESA), (b) Energy Transfer Upconversion (ETU), (c) Photon Avalanche (PA), (d) Cooperative Energy Transfer (CET).

1.4.2.2.(i) Ground/Excited State Absorption (GSA/ESA)

The Ground/Excited State Absorption (GSA/ESA) process involves the absorption of low-energy photons, which is possible if the material has an adequate absorption cross-section to interact with the incident radiation. This phenomenon was first observed by N. Bloembergen in 1959 in rare-earth and transition metal salts embedded in a lattice host, where successive absorption of near-infrared (NIR) photons occurs. The process was later confirmed by Auzel's upconversion (UC) experiments after invention of laser. The ESA process is similar to the GSA process, except that the atoms must remain in the excited state for a longer period to facilitate the absorption of additional photons. The absorption cross-section of the intermediate state must also be sufficiently large to interact with the incoming photons. Fortunately, the intermediate metastable states of Ln^{3+} ions meet this requirement. The UC process can be explained using a three-level energy diagram (as shown in Fig 1.4(a))**.** When a beam of resonant photons (phonon-assisted transfer) with energy ΔE ($E_2 – E_1$) interacts with the sample, ions in the ground state (E_1) are promoted to the excited state (E_2) via the GSA process. If E_2 is a metastable state, the ions will absorb another photon before relaxing back to the ground state, reaching a higher energy state, E_3. However, the successive absorption of photons depends on the population density in the excited state. Finally, when the ion

transitions from E_3 to the ground state, a photon is emitted with higher energy than the incident photons.

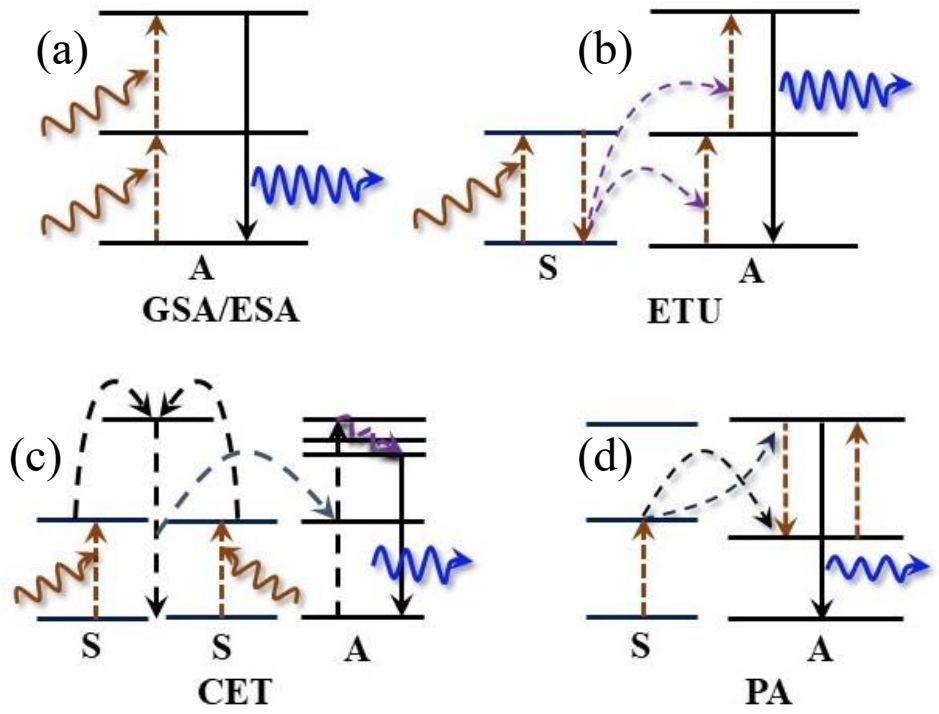

*Figure 1.4 Various energy transfer mechanisms **(a)** Ground/Excited State Absorption (GSA/ESA), **(b)** Energy Transfer Upconversion (ETU), **(c)** Cooperative Energy Transfer (CET). **(d)** Photon Avalanche (PA)*

1.4.2.2.(ii) Energy transfer upconversion (ETU)

Lanthanides, when used as luminescent centres, typically exhibit weak upconversion (UC) due to the minimal absorption cross-section for near-infrared (NIR) photons by their intermediate states, unless efficiently sensitized by a nearby source. The Energy Transfer Upconversion (ETU) process is widely prevalent mechanism in UC emission, was first identified by Auzel in systems involving pairs of Ln^{3+} ions, such as Yb^{3+}-Er^{3+} and Yb^{3+}-Tm^{3+} in solids. In these systems, one dopant functions as a sensitizer while the other acts as an activator. For effective UC, the sensitizer's absorption cross-section must be much larger than that of the activator. ETU is an energy transfer process where sensitizer ions, typically doped

at higher concentrations absorbed NIR photons and then efficiently transfer energy to nearby activator ions. This mechanism can be visualized using an energy level diagram (Fig 1.4(b)), where activator ions are excited through energy transfer from both the ground and excited states of the sensitizer ions.

1.4.2.2.(iii) Cooperative Energy Transfer (CET)

Cooperative energy transfer (CET) typically involves the simultaneous excitation of a pair of adjacent sensitizer ions through virtual states, which then transfer their combined energy to a single activator ion. This process is similar to energy transfer upconversion (ETU) but excludes the involvement of real metastable energy states for UC process. The direct excitation of an activator ion without involving the intermediate metastable states requires comparatively higher excitation power density. Consequently, CET emission efficiency is generally lower than that of ETU. The mechanism of CET is illustrated in the energy level diagram shown in Fig 1.4(c). In this process, the neighbouring sensitizer ions (S1 and S2) absorb low-energy photons and transfer their energy directly to the activator ion. CET typically occurs in fluorescent materials where the energy provided by a sensitizer ion is exactly half of the energy required to excite the activator ion.

1.4.2.2.(iv) Photon Avalanche (PA)

The photon avalanche (PA) process in Ln^{3+}-doped materials leads to a significant enhancement in emission intensity, often surpassing that of normal upconversion (UC) under specific conditions. This phenomenon was first observed by Chivian in 1979 in Pr^{3+}-doped $LaCl_3$ and $LaBr_3$ materials. In Ln^{3+} ions, phonon-assisted ground-state absorption typically occurs due to the energy mismatch with the pump photon. The PA mechanism can be explained using a three-energy-level system, as illustrated in Fig 1.4(d)**.** In this model, ions

are initially excited to an intermediate state. Subsequently, an excited-state absorption (ESA) process promotes ions to a higher excited state, where relaxation follows the standard UC process. If the energy gap between the ground state and the intermediate state is resonant with the pump photon energy, resonant cross-relaxation can occur between ions in the higher excited states and neighbouring ions in the ground state. This interaction produces two ions in the intermediate state, leading to an exponential increase in the intermediate-state population and a sudden enhancement in UC efficiency. Achieving this effect requires the pump power to exceed a certain threshold (threshold power density).

1.5 Lanthanides activated luminescent materials

Phosphors are solid materials that emit visible light when they absorb energy from various sources, such as optical, electrical, mechanical, or thermal stimuli. This phenomenon, known as luminescence, can manifest in the forms of fluorescence or phosphorescence, with the emitted photons spanning a range of wavelengths from ultraviolet to visible, and in some cases, infrared, depending on the material's electronic structure. The phenomenon of photo-emission typically involves the excitation of electrons within a material to higher energy states, followed by their relaxation to the ground state, during which energy is released as photons. However, a fundamental question in this domain is the underlying mechanism by which photoluminescence is generated in phosphors.

Traditionally, phosphors are understood to consist of inorganic host materials, which may be either self-activated or doped with impurities, typically transition metals, that induce photoluminescent properties. Self-activated inorganic phosphors exhibit photoluminescence through intrinsic electronic transitions within the host material, relying on defect states, charge transfer states, or localized electronic levels to absorb energy and release it as light,

eliminating the need for external dopants. Common examples include composite materials such as metal oxide and sulfide-based compounds, where luminescence is associated with native defects or electron-hole pair recombination. In contrast, transition metal-doped inorganic phosphors, such as those incorporating manganese (Mn), chromium (Cr), or zinc (Zn), are widely used for their abundant electronic structures, with these metals introducing specific electronic states that facilitate efficient energy absorption and emission. The characteristics of the emitted light, whether it is broad or narrow, short-lived or persistent, are determined by the material's electronic properties, which result from the interactions between the host lattice and any dopants or intrinsic defects within the material. These materials often exhibit broad, intense emission spectra due to the intrinsic electronic transitions or between the d-orbitals of the transition metal ions. Both self-activated and doped photo-activated inorganic materials are often cost-effective and simpler to synthesize, yet they are more susceptible to non-radiative decay mechanisms, which can reduce their overall photoluminescence efficiency.

Lanthanide luminescence, similar to transition metal-doped hosts, involves the incorporation of Ln-ions into stable inorganic lattices (typically made of oxides, fluorides, or phosphates). These lanthanide ions absorb external photons and emit light through specific intra 4f-4f or 4f-5d electronic transitions, resulting in sharp, narrow emission lines with high spectral purity. The host material is crucial for activating and enhancing lanthanide emission, as it provides a stable, non-centrosymmetric environment that enables efficient energy transfer to the lanthanide ions. Although intra-4f-4f transitions are generally forbidden by the Laporte rule, the crystalline field host materials, which incorporates lanthanide ions at specific sites, either by substituting metal ions or occupying interstitial sites, helps alleviate this

restriction and make partially allowed 4f-4f transitions. Furthermore, the host's structure isolates the lanthanide ions, minimizing quenching from non-radiative processes and thereby improving luminescent efficiency. In addition to acting as an energy transfer medium, the host material can also absorb energy from external sources (such as ultraviolet or visible light) and transfer it to the lanthanide ions, further promoting luminescence.

In addition to traditional Ln-activated inorganic phosphors, lanthanide-doped organic phosphors, including organic complexes, lanthanide-activated metal-organic frameworks (MOFs), and other hybrid materials, have also emerged as promising candidates for advanced luminescent applications. In typical organic complexes, lanthanide ions coordinate with organic ligands, enabling efficient energy transfer to the lanthanide through the antenna effect. This process is often strategically designed to optimize energy transfer and thereby enhance luminescence efficiency. Lanthanide-doped MOFs, which are crystalline materials composed of metal ions or clusters connected by organic ligands, offer a highly ordered and porous structure, making them excellent for luminescence applications. The lanthanide ions embedded in these frameworks provide highly stable luminescent centres, while the organic ligands allow for fine-tuning of the emission properties, such as colour and intensity. One of the key advantages of lanthanide-doped organic phosphors is their versatility and ease of fabrication. Unlike inorganic phosphors, which often require high-temperature synthesis, lanthanide-doped organic materials can be synthesized under milder conditions, offering greater flexibility in device fabrication and potential for large-scale production. Moreover, the organic components can introduce additional functionalities, such as solubility in organic solvents, improved processability, and the potential for creating flexible or lightweight luminescent devices. In applications like organic light-emitting diodes (OLEDs), solar cells,

and sensors, lanthanide-doped organic phosphors provide significant improvements in performance, including enhanced luminescence efficiency, stability, and tunability. Collectively, the host material (Inorganic/organics) provides the essential structural and electronic framework required for efficient lanthanide luminescence, making lanthanide-doped phosphors particularly well-suited for a wide range of applications, including lighting, displays, LEDs and lasers.

The efficiency of lanthanide emission is influenced by several critical factors, including the properties of the host material, temperature effects, energy transfer mechanisms, sensitization, multiphonon relaxation, and dopant concentration. Optimizing these factors is crucial for enhancing the luminescent performance and stability of lanthanide-doped phosphors in diverse applications. Among these, multiphonon relaxation and concentration quenching are particularly important to examine, as they have a significant impact on emission efficiency.

1.5.1 Multi-phonon Relaxation in Solids

In solid-state systems, the process by which an excited dopant atom or ion returns to its ground state involves both radiative and non-radiative relaxation pathways. Radiative relaxation involves the emission of photons, whereas non-radiative relaxation transfers energy to the crystal lattice as phonons. This non-radiative decay process, often called multiphonon relaxation, is crucial in determining the efficiency of luminescent materials, particularly lanthanide-doped phosphors where electron-phonon coupling within the lattice influences relaxation rates [22]. When an excited electron undergoes non-radiative decay, energy is transferred to the host lattice through phonons quantized lattice vibrations. If the energy gap (ΔE) between electronic states is significantly larger than the energy of a single phonon,

multiple phonons can be emitted simultaneously. This process is known as multiphonon relaxation. The rate of multiphonon relaxation is influenced by the electron-phonon coupling strength and the phonon energy of the host lattice. When the energy gap between states is much larger than the energy of a single phonon, the multiphonon decay rate Wp can be expressed as[23]:

$$W_p = C(n(T)+1)^p \exp[-p\, ln(\varepsilon)] \qquad \ldots (1.4)$$

C is a material-specific constant, In (ε) is another constant that varies with the host lattice, $n(t) = \left(\exp^{\left(\frac{\hbar\omega}{k}t\right)} - 1\right)^{-1}$ represents the phonon occupancy factor (its value is less than 1), and p denotes the number of phonons involved in the process. The decay rate increases exponentially as the number of phonons required for energy relaxation increases. Typically, radiative transitions are substantially suppressed if the energy gap between states is less than the equivalent of four to five phonon energies, while larger gaps (over five phonon energies) favor radiative processes due to reduced phonon interaction.

1.5.2 Concentration Quenching

Concentration quenching is a phenomenon observed in phosphor materials when the emission intensity decreases as the dopant concentration increases beyond a critical value. This effect is critical in optimizing dopant concentration to achieve maximum luminescence efficiency in lanthanide-activated phosphors. When the concentration of dopant ions is high, energy transfer between neighboring ions becomes more frequent, reducing the distance between activator ions below a critical level [24]. This increased proximity leads to energy migration through the lattice until it encounters "killer" sites defects or impurities where the energy is lost non-radiatively. This process was explained by Dexter and Schulman (1954),

who proposed that excessive dopant concentration promotes energy transfer to defect sites, which act as quenching centers [25]. Cross-relaxation processes, where two neighboring ions exchange energy such that one ion reaches a lower-energy state, also contribute to concentration quenching and decrease luminescence efficiency.

1.6 Introduction to Upconverting Nanoparticles (UCNPs)

The remarkable upconversion properties inherent to lanthanide ions enable the design of upconverting nanoparticles (UCNPs), which are typically crafted with diameters less than 100 nm. These NPs consist of a host matrix embedded with rare earth ions, which serve as the emission centres under near-infrared (NIR) excitation, enabling the efficient conversion of low-energy photons, such as NIR light, into higher-energy emissions like ultraviolet or visible photons. Such small-sized nanoparticles are ideal for a variety of advanced applications, including bioimaging, sensing, lasing, photo switching and energy harvesting *etc*., due to their tunable optical properties, high surface area, and stability in complex environments. Although other luminescent materials, including fluorescent organic dyes, organic complexes, inorganic compounds, and quantum dots, show considerable potential but their practical applications are often limited by factors such as poor photostability, toxicity, broad absorption and emission spectra, and relatively moderate quantum yields [26].

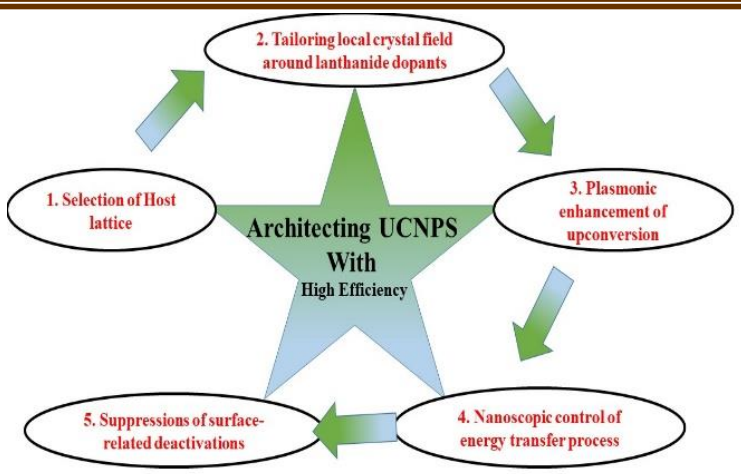

Figure 1.5 General strategies to achieve the high efficiency of UCNPs

In contrast, UCNPs exhibit a range of exceptional properties that make them highly suitable for advanced application, offering a more efficient alternative over traditional phosphor materials. For instance, these include lower toxicity, less autofluorescence, minimal photobleaching, narrow band emission and also extended decay time, which is particularly advantageous for bioimaging. UCNPs also offer a high conversion efficiency. the ability to generate multicolour emission from a single excitation source, colour turnability, an improved signal-to-noise ratio and significant anti-Stokes shifts, further enhancing their utility in various optoelectronic devices [27][28]. The emission properties of UCNPs are influenced by factors such as the choice of dopant ions, the energy transfer efficiency of the host matrix, excitation wavelength and intensity, particle size, and surface coatings. To optimize radiative upconversion emissions, a low-vibrational-energy host material is typically selected to minimize non-radiative losses. Fig 1.5 illustrates several strategies developed to improve the UC efficiency of UCNPs. Apart from that Due to the high surface-to-volume ratio of UCNPs, dopant ions located near the nanoparticle surface are often subject to emission quenching from interactions with surface defects or impurities, which can reduce overall upconversion

efficiency. To mitigate these surface-related losses and enhance conversion, various surface engineering strategies have been developed, including the design of homogeneous and heterogeneous core@shell structures, active core/active shell configurations, and the incorporation of plasmonic enhancements [26][28]. These engineering strategies are crucial for harnessing the full potential of UCNPs in a wide range of applications, including sensing, bioimaging, and photonic devices.

1.7 Characterization of Calcium Molybdate [$CaMoO_4$] as a Host Material

Calcium molybdate ($CaMoO_4$) is a versatile host material for incorporating lanthanides, enabling efficient harvesting of their optical properties. It offers key advantages, including low phonon energy, a wide optical bandgap, and a stable crystal structure, which together create an optimal environment for energy transfer with minimal non-radiative losses. In addition, $CaMoO_4$ serves as an economically viable host material and can be readily synthesized using various cost-effective methods, such as solid-state reactions, sol-gel processes, hydrothermal/solvothermal techniques etc, thereby making it suitable for both research applications and large-scale industrial production. The material's high melting point, non-hygroscopic nature, and high refractive index further enhance its robustness, ensuring stability under challenging conditions, including exposure to moisture, acids, and high temperatures. This stability ensures that $CaMoO_4$-based luminescent materials maintain their performance over time, making them suitable for long-term use in applications. These attributes, along with its scalability, thermal stability, and tunable optical properties, make $CaMoO_4$ an exceptionally promising material for applications in temperature sensing, latent

fingerprint detection, and optoelectronic devices, thereby enhancing its significance in advanced technological and photonic fields.

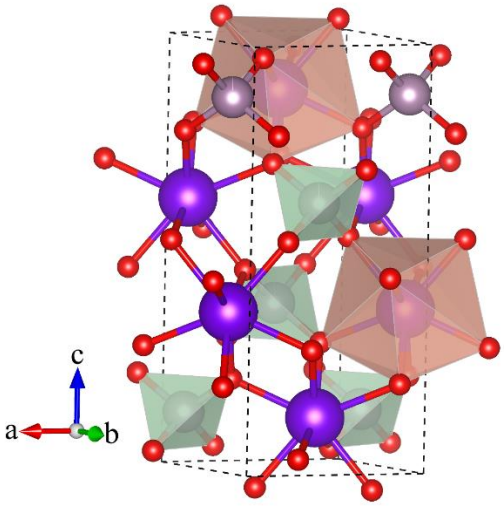

Figure 1.6 Schematic illustrating the crystal structure of tetragonal $CaMoO_4$.

$CaMoO_4$ belongs to the scheelite family of compounds and features a tetragonal crystal structure with the space group $I4_{1/a}$. Scheelite-type ABO_4 compounds (where A can be an alkali metal, Ca^{2+}, Sr^{2+}, Ba^{2+}, or Bi^{3+}, and B can be Mo^{6+} or W^{6+}) are widely used in various functional applications, including scintillation detectors, phosphors, lasers, photocatalysts, and lithium-ion batteries [29]. In calcium molybdate ($CaMoO_4$), the Ca^{2+} ions are coordinated to eight oxygen atoms, forming a distorted dodecahedron [CaO_8] structure, while the Mo^{6+} ions are surrounded by four oxygen atoms, resulting in a tetrahedron (MoO_4) structure connect by sharing vertices and oxygen atoms, as illustrated in Fig 1.6. Although the lanthanide emission is strongly influenced by the crystalline field of host, which splits the degenerate energy levels of the ion, affecting transition probabilities and emission intensity. The phonon frequencies of the host material determine the efficiency of non-radiative relaxation, with higher phonon energies increasing the likelihood of quenching emissions. A balance between crystalline field strength and phonon energy is crucial for optimizing the radiative emission

and lifetime of lanthanide ions in solid-state materials. The exponential energy gap law defines the rate of nonradiative relaxation in solids, which is given by

$$k_{nr} = \beta_{de} \exp\left(-\alpha(\Delta E - 2\hbar\omega_{max})\right) \qquad \ldots (1.5)$$

Where, β_{de} and α are constants specific to the host lattice, ΔE represents the energy difference between the involved levels, and $\hbar\omega_{max}$ denotes the maximum phonon energy of the host. $CaMoO_4$, with its relatively low phonon energy of approximately 800 cm^{-1}, significantly reduces the probability of nonradiative transitions, resulting in enhanced luminescence efficiency compared to other hosts with higher phonon frequencies. Table 1.5 presents a comparison of the phonon energies for various host materials.

Table 1.5 Energy of the maximum phonon frequency for different hosts [30].

Materials	**Phonon Vibration (cm^{-1})**
Borate	1400
Phosphate	1100
Silicate	1000–1100
Germanate	800–975
$CaMoO_4$	800
$Y_2TI_2O_7$	712
Tellurite	600–850
Y_2O_3	550
YVO_4	600
Fluoride	500–600
$LaCl_3$	260
Bromide	175–190
$LaBr_3$	175
Iodide	160

The photoluminescence (PL) properties of $CaMoO_4$ are particularly intriguing due to its unique electronic structure, which gives rise to distinctive luminescent behavior, often referred to as self-activated emission. The absorption spectrum of pure $CaMoO_4$ exhibits strong absorption in the UV region (200–300 nm), attributed to electronic transitions across its wide bandgap, with UV absorption primarily associated with charge transfer bands involving Mo^{6+}–O^{2-} interactions. In contrast, absorption decreases significantly in the visible (400–700 nm) and near-infrared regions, highlighting its transparency in these regions. A distinct absorption edge, characteristic of its wide bandgap, marks the onset of light absorption. With a direct bandgap of around 4.2 eV, $CaMoO_4$ remains transparent in the visible range while absorbing high-energy UV radiation with wavelengths shorter than 350 nm. Notably, doping with lanthanides significantly alters the bandgap by introducing localized energy states within it. In calcium molybdate, both ligand-to-metal charge transfer (LMCT) and metal-to-ligand charge transfer (MLCT) contribute to its broad emission spectrum. Upon UV excitation, electrons in the oxygen ligands (O^{2-}) are excited to higher energy levels within the molybdenum (Mo) center, initiating LMCT. This transfer of electron density from the oxygen ligands to the molybdenum metal causes electronic reorganization within the Mo centre, which is linked to the observed absorption. Additionally, MLCT involves the transfer of charge from the molybdenum back to the oxygen ligands, further shaping the emission profile and enhancing the material's luminescent properties. These charge transfer processes play a crucial role in determining the emission profile of the host material and are sometimes used to facilitate efficient energy transfer to dopants. Additionally, the luminescence efficiency of $CaMoO_4$ is influenced by factors such as particle size, morphology, and purity, which impact both radiative and non-radiative processes. By

optimizing these parameters, the luminescent efficiency and color purity of $CaMoO_4$ can be enhanced, making it a promising candidate for next-generation phosphor applications. The photoluminescence excitation (PLE) and photoluminescence (PL) spectra of $CaMoO_4$ are shown in Fig 1.7. The excitation spectra of pure $CaMoO_4$ displaying strong excitation near 290 nm, with emission centred around 500 nm, covering almost the entire visible region.

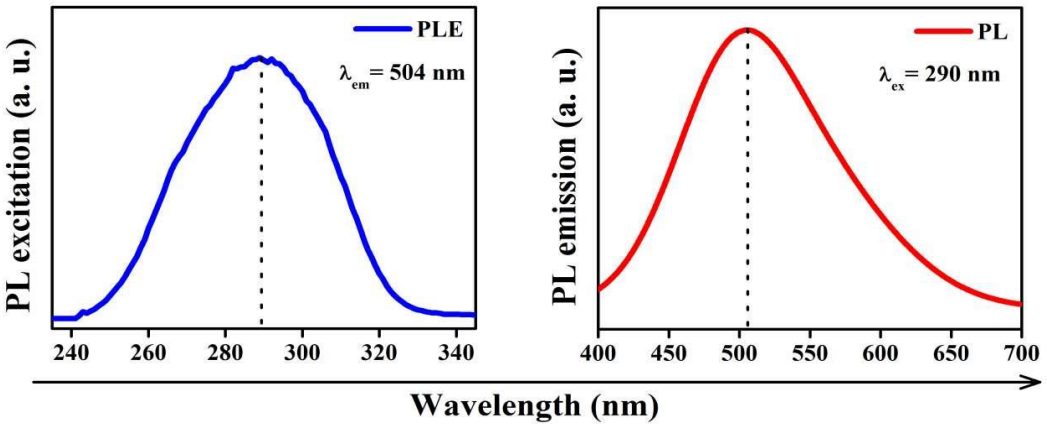

Figure 1.7 The PLE and PL spectrum of $CaMoO_4$ Phosphor.

The extraction of lanthanide emission in a host material such as $CaMoO_4$ (calcium molybdate) entails the incorporation of lanthanide ions (e.g., Er^{3+}, Ho^{3+}, Tm^{3+} or Yb^{3+}) into the crystal lattice through a doping process. This is typically achieved by substituting Ca^{2+} ions with lanthanide ions or by introducing small amounts of lanthanide dopants during the synthesis, ensuring their integration within the host structure. Common synthesis methods, such as solid-state reactions, sol-gel processes, or hydrothermal synthesis, ensure that lanthanide ions are uniformly incorporated into the crystal structure of $CaMoO_4$. Lanthanide ions exhibit sharp, well-defined emission spectra due to f-f electronic transitions, which are minimally affected by environmental changes. Their thermal stability in materials like $CaMoO_4$ helps prevent thermal quenching, while energy transfer mechanisms and tunable

emissions enable versatile applications in lighting, multi-color displays, and LEDs. Additionally, their sensitivity to environmental changes ensures stable performance in demanding applications like lasers and displays.

1.8 Application of Ln^{3+} activated $CaMoO_4$ phosphors

Ln^{3+}-doped $CaMoO_4$ phosphors have garnered significant interest for their multifaceted applications, owing to their exceptional luminescent properties, structural stability, and emission tunability. By doping with different rare earth ions (Eu^{3+}, Tb^{3+}, Dy^{3+}, Er^{3+}, Tm^{3+}, Yb^{3+}), these materials find utility across lighting, sensing, displays, and other advanced technological domains.

(a) Lighting and Display Applications: Ln^{3+}-doped $CaMoO_4$ phosphors are pivotal in lighting and display technologies due to their tunable emission colors ranging from blue-green to orange-red. For instance, $CaMoO_4$:Eu^{3+}, Tb^{3+}, Dy^{3+} nanofibers fabricated via sol-gel and electrospinning processes demonstrate tunable luminescence resulting from efficient energy transfer from molybdate groups to dopants, making them suitable for fluorescent lamps and field emission displays [31]. Co-doping with Mn^{2+} has further enhanced red luminescence in $CaMoO_4$:Eu^{3+} phosphors, enabling their use in warm white light-emitting diodes (LEDs), crucial for energy-efficient lighting systems [32]. Similarly, Dy^{3+}/Sm^{3+} co-doped $CaMoO_4$ phosphors achieve neutral white light emission with a correlated color temperature of 4439 K, making them ideal for white lighting diode applications [33]. K^+-compensated $CaMoO_4$:Dy^{3+} nanophosphors exhibit bright yellow and blue emissions with enhanced photoluminescence, further broadening their applications in white LED technologies [34].

(b) Temperature Sensing and Optical Thermometry: The temperature-dependent luminescence properties of Ln^{3+}-doped $CaMoO_4$ phosphors make them suitable for optical thermometry and contactless temperature sensing. Er^{3+}-Tm^{3+}-Yb^{3+}: $CaMoO_4$ phosphors exhibit outstanding upconversion-based optical temperature sensing, achieving a maximum sensor sensitivity of 0.0182 K^{-1} at 413 K. These materials are also capable of laser-induced optical heating, expanding their applicability in advanced sensing technologies [35]. Co-doping strategies, such as Bi^{3+} co-doping in $CaMoO_4$: Er^{3+}/Yb^{3+}, have significantly enhanced upconversion emission intensity (by ~25 times) and improved temperature sensing performance. This enhancement is attributed to local symmetry distortion and a reduction in non-radiative channels, demonstrating their potential for high-sensitivity temperature monitoring [36].

(c) Photocatalysis and Environmental Applications: Ln^{3+}-doped $CaMoO_4$ phosphors exhibit remarkable photocatalytic activity. For example, SDS-stabilized $CaMoO_4$:Ln^{3+} nanocrystals (Ln^{3+} = Eu^{3+}, Er^{3+}/Yb^{3+}) synthesized via microwave methods have demonstrated strong photocatalytic properties, including an ~80% degradation of Rhodamine B dye under UV illumination. These findings highlight their potential in environmental remediation and water purification.

(d) Transparent Photoluminescent Films and Sensors: Ln^{3+}-doped $CaMoO_4$ phosphors also find applications in photoluminescent films and advanced sensor technologies. Silica-modified $CaMoO_4@SiO_2$:Ln^{3+} (Ln^{3+}= Eu^{3+}, Tb^{3+}, Dy^{3+}) phosphors exhibit enhanced emission intensity, enabling their use in transparent films and LED devices. These phosphors have also been explored for selective detection of dichromate ions, showcasing their utility in analytical sensing applications [37].

(e) Advancements in Upconversion Luminescence: Ln^{3+}-doped $CaMoO_4$ materials demonstrate robust upconversion luminescence, making them suitable for cutting-edge optical technologies. For example, $CaMoO_4$: Er^{3+}/Yb^{3+} phosphors exhibit efficient energy transfer processes that enable visible emissions under near-infrared excitation, a feature critical for developing optical heaters and bioimaging probes. Additionally, their ability to tune emissions via co-doping strategies makes them versatile for diverse applications.

(f) Challenges and Future Directions: Despite significant advancements, challenges remain in optimizing the performance of Ln^{3+}-doped $CaMoO_4$ phosphors. Thermal quenching, limited quantum efficiency, and host material compatibility in certain applications require further research. Innovations in co-doping strategies, surface modifications, and host lattice engineering are paving the way for next-generation phosphors with superior efficiency and functionality. In conclusion, Ln^{3+}-doped $CaMoO_4$ phosphors exhibit exceptional versatility, making them indispensable in lighting, sensing, environmental, and optical technologies. Continued research into their luminescent properties and functional enhancements will further expand their applicability across emerging fields.

1.8.1 Temperature sensing

Temperature sensing is essential across various scientific and industrial fields, from monitoring environmental changes to ensuring precision in biomedical applications. Despite their widespread use, conventional sensors such as thermometers, thermocouples, RTDs, and thermistors exhibit notable limitations, particularly under extreme conditions or in dynamic systems. These sensors typically rely on direct contact with the measurement surface, which restricts their use in challenging environments such as power plants, oil refineries, fire detection systems, and biological fluids, where rapid changes, hazardous conditions, or

inaccessibility pose significant challenges [38][39]. The demand for advanced, precise, and contactless temperature measurement techniques has driven research into non-invasive thermal sensing technologies. Among these, lanthanide-doped optical materials, especially $CaMoO_4$, have demonstrated significant potential [36]. Lanthanide-doped materials, including those with ions like Er^{3+}, Ho^{3+}, Tm^{3+}, and Yb^{3+}, exhibit unique temperature-sensitive luminescent properties, enabling the development of ratiometric thermometers for highly accurate temperature measurement. These materials use the temperature-dependent luminescence of lanthanide ions to enable precise, contactless temperature measurements, which is especially valuable when direct contact is impractical or undesirable.

Among non-contact methods, luminescent thermometry is distinguished by its high spatial and thermal resolution, fast response time, and non-invasive nature, making it especially well-suited for advanced applications in challenging environments. The concept of luminescent thermometry, initially introduced by Kusama in 1976, has since advanced to encompass various techniques, including band-shape, spectral, polarization, bandwidth, and decay time measurements, with the most prominent being fluorescence intensity ratio (LIR) thermometry [40]. The fluorescence intensity ratio (FIR) method, in particular, has garnered attention for its resistance to variations in excitation intensity and transmission losses, enabling more stable and accurate temperature measurements. Recent advancements, such as the device by Edinburgh Instruments using $NaYF_4$: Yb^{3+}/Er^{3+} phosphors with 1.0% K^{-1} sensitivity, highlight the practicality and precision of luminescent thermometry. In FIR-based thermometry, the temperature is determined by observing the intensity ratio between two emission bands, which may arise from different energy levels of the same dopant or distinct dopants. This temperature-sensitive behaviour is attributed to nonradiative transitions, where

higher temperatures typically increase nonradiative decay rates, leading to changes in emission intensity. In the LIR technique, usually, two approaches, thermally coupled levels (when the separation between energy levels lies in the region of 200 – 2000 cm^{-1}) and non-thermally coupled levels (when the separation between energy levels is more than 2000 cm^{-1}), are used for the optical thermometry. In FIR-based thermometry, temperature is determined by examining the intensity ratio between two emission bands, which may stem from either different energy levels of a single dopant or from different dopants, while maintaining adequate spatial resolution. The temperature-dependent behaviour is mainly driven by nonradiative transitions, where higher temperatures generally accelerate nonradiative decay rates, resulting in thermal quenching and shifts in population distribution, which in turn cause changes in emission intensity. The FIR method generally employs two distinct strategies: (a) Thermally Coupled Levels (TCLs), where the energy gap between the coupled states is between 200 and 2000 cm^{-1}, and (b) Non-Thermally Coupled Levels (NTCLs), where the energy separation between the emitting states surpasses 2000 cm^{-1}. Both approaches are effectively utilized in optical thermometry [41][42].

1.8.1.1 *Theoretical background of temperature sensing based on TCLs*

Lanthanide ions are well known for their complex electronic structures, which give rise to distinct energy states that are often thermally coupled. Some notable examples of Ln^{3+} ions exhibiting thermally coupled levels, including $Er^{3+}(^4S_{3/2}/^2H_{11/2})$, $Ho^{3+}(^5F_4/^5S_2)$, Nd^{3+} $(^4F_{7/2}/^4F_{5/2})$, $Tm^{3+}(^3F_{2,3}/^3H_4)$, are commonly employed in temperature-sensing applications due to their distinctive thermally sensitive emission properties. Thermally coupled levels (TCLs) describe excited states of lanthanide ions that are energetically proximate (typically 200 to 2000 cm^{-1}), allowing thermal excitation to facilitate transitions between these states.

The redistribution of populations between these levels is temperature-dependent and is governed by Maxwell-Boltzmann statistics, providing a mathematical framework to model the thermal population shifts. To understand the mechanism of thermally induced population shifts in thermally coupled levels (TCLs), we consider a three-level system, where the energy levels are labelled E_0, E_1, and E_2, with corresponding population densities N_0, N_1, and N_2, as shown in Fig. 1.8.

The luminescence intensity corresponding to a specific emission band is directly proportional to the number of excited ions or atoms occupying the respective energy level. Consequently, the fluorescent intensity ratio (FIR) for these levels can be written as [43]:

$$FIR = \frac{I_2}{I_1} = \frac{N_2}{N_1} = \frac{W_2 g_2 h\nu_2}{W_1 g_1 h\nu_1} exp\left(\frac{-\Delta E}{k_B T}\right) = C exp\left(\frac{-\Delta E}{k_B T}\right) \quad \ldots (1.5)$$

where C= $\frac{W_2 g_2 h\nu_2}{W_1 g_1 h\nu_1}$ is a pre-exponential factor, with I_i, k_B, g_i, W_i, and $h\nu_i$ representing the luminescence intensity, Boltzmann constant, degeneracy, emission cross-section, and angular frequency associated with the i^{th} level, respectively. Here, ΔE is the energy gap between the thermally coupled levels.

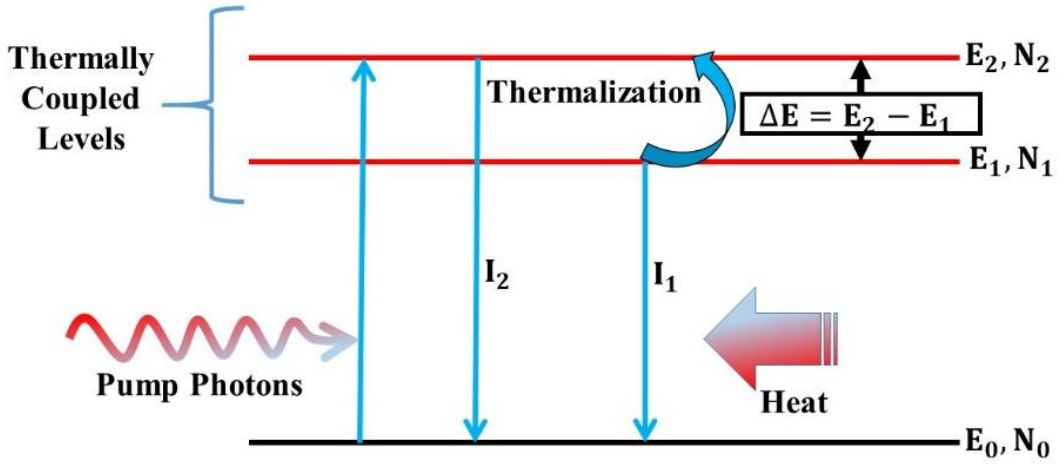

Figure 1.8 Schematic diagram showing TCLs based thermalization process.

Assessment of temperature sensing capabilities, it is essential to define two fundamental parameters; Absolute sensitivity (Sa) and Relative sensitivity (Sr). Absolute sensitivity (Sa) measures the rate of change in the fluorescent intensity ratio (FIR) relative to temperature in absolute terms. It is commonly used to compare the sensitivity of materials of the same type. In contrast, relative sensitivity (Sr) normalizes this rate by the current FIR value, yielding a dimensionless measure of sensitivity, which is primarily used for comparing the sensitivity across different types of materials. The mathematical formulation of Sa and Sr is provided by the following relations:

$$S_a = \frac{\partial(FIR)}{\partial T} = FIR \times \frac{\Delta E}{k_B T^2} \; and \; S_r = \frac{1}{(FIR)} \times \frac{\partial(FIR)}{\partial T} = \frac{\Delta E}{k_B T^2} \qquad \ldots (1.6)$$

These expressions indicate that both absolute sensitivity (S_a) and relative sensitivity (S_r) are directly influenced by the energy gap (ΔE) between the TCLs. The value of ΔE is influenced by factors such as the type of dopants, the host matrix, and the interaction between the host and the dopants. While significant progress has been made in contactless optical thermometry using TCL-FIR techniques with inorganic phosphors, challenges remain, particularly in achieving high sensitivity across a wide temperature range due to the narrow ΔE of conventional methods. Additionally, the application of this technique to systems with dual luminescent centers is complicated by deviations from the simple Boltzmann population distribution model, limiting its effectiveness. To address these limitations, the exploration of non-thermally coupled levels (NTCL) mechanisms has emerged as a promising alternative, offering potential solutions for more versatile and sensitive temperature sensing.

1.8.1.2 *Theoretical background of temperature sensing based on NTCLs*

An alternative method for temperature measurement is the non-thermally coupled levels (NTCL)-based Fluorescence Intensity Ratio (FIR) technique, which offers enhanced sensitivity and broader applicability, even in systems with dual luminescent centres [44][45]. In this approach, two emitting states, either from the same dopant or from two distinct luminescent centres, are selected, with an energy separation typically greater than 2000 cm^{-1}. In such systems, the temperature-dependent luminescence arises from the intrinsic properties of the host material, with population redistribution occurring due to thermal agitation. To derive the temperature-sensing parameters using this technique, the basic framework remains similar to that of traditional TCLs, but the observed FIR is no longer governed by the Boltzmann distribution law. Instead, a suitable equation, such as a polynomial equation, Stern-Volmer relation (for dual luminescent centres), modified Arrhenius equation, or Boltzmann sigmoidal function, etc. is applied to fit the observed FIR data. The fitted equation is then differentiated with respect to temperature to determine the sensing parameters, such as absolute sensitivity (S_a) and relative sensitivity (S_r). This procedure is followed for fitting each type of function to estimate the sensing parameters.

In this study, to demonstrate NTCLs-based temperature sensing, for example, FIR fitting is performed using the Arrhenius equation, after which the sensing parameters are calculated as shown below [46]:

$$I(T) = \frac{I_0}{1 + \mathrm{A}\exp\left(-\frac{E_a}{kT}\right)} \qquad \ldots (1.7)$$

Here, I_0 and $I(T)$ denote the initial luminescence intensity and the intensity at temperature *T*, respectively. *A* is the pre-exponential constant, *k* is the Boltzmann constant, and E_a represents the activation energy. For different emitting levels, the temperature-dependent luminescence intensities can be represented as follows:

$$I(T)'_1 = \frac{I'_{0,1}}{1 + A_1 \exp\left(-\frac{E'_{a,1}}{kT}\right)} \,\&\, I(T)'_2 = \frac{I'_{0,2}}{1 + A_2 \exp\left(-\frac{E'_{a,2}}{kT}\right)} \quad \ldots (1.8)$$

Thus, the FIR can be approximated as:

$$FIR = \frac{I(T)'_2}{I(T)'_1} = \frac{I'_{0,2}}{I'_{0,1}} \frac{1 + A_1 \exp\left(-\frac{E'_{a,1}}{kT}\right)}{1 + A_2 \exp\left(-\frac{E'_{a,2}}{kT}\right)} \approx \alpha + \beta \exp\left(\frac{-\Delta E_a}{kT}\right) \quad \ldots (1.9)$$

where α, β , and ΔE_a are parameters related to the selected energy levels, which can be determined from a plot of FIR *versus* T using the above expression. Further, the absolute sensitivity S_a and relative sensitivity S_r for temperature sensing can be defined as:

$$S_a = \left|\frac{\partial LIR}{\partial T}\right| = \frac{\Delta E_a}{kT^2} \beta \exp\left(\frac{-\Delta E_a}{kT}\right) \qquad \ldots (1.10)$$

$$S_r = \left|\frac{1}{LIR}\frac{\partial LIR}{\partial T}\right| = \frac{\Delta E_a}{kT^2} \frac{\beta \exp\left(\frac{-\Delta E_a}{kT}\right)}{\alpha + \beta \exp\left(\frac{-\Delta E_a}{kT}\right)} \ldots (1.11)$$

Equations 1.13 and 1.14 outline the sensing parameters, Sa and Sr, in NTCL-FIR based temperature sensing, forming a foundational framework for optical thermometry. These fitting equations are crucial for deriving the sensing parameters and for understanding the temperature-dependent behaviour of the luminescent material. Additionally, various mathematical models have been employed in NTCL-FIR-based studies to advance contactless

optical thermometry applications. The NTCL-FIR technique offers two distinct advantages over the TCL-FIR method: it provides higher sensitivity (with enhanced Sa and Sr values) and greater accuracy.

1.8.2 LFP Detection Using Luminescent Materials through Powder Dusting method

1.8.2.1 *LFPs detection techniques*

Latent fingerprint detection is a crucial process in forensic science and law enforcement, used to identify individuals through the unique ridge patterns left on surfaces. Fingerprints are particularly reliable for identification due to their permanence and uniqueness, with each person possessing a distinct pattern of ridges and valleys, even among identical twins. These invisible impressions are formed when oils, sweat, or other substances from the skin come into contact with an object. Though not visible to the naked eye, latent prints can be revealed using various techniques such as powder dusting, chemical treatments, or alternate light sources. Given their uniqueness, fingerprints play a vital role in linking individuals to crime scenes, solving cases, and identifying people in both criminal and non-criminal contexts.

Fingerprint recognition systems, like the Automated Fingerprint Identification System (AFIS), optimize fingerprint storage and comparison, enabling fast and efficient searches across large databases. AFIS digitizes fingerprint images and evaluates key characteristics such as sharpness (clear ridge details), contrast (distinctive patterns), and size (features like arches, loops, and whorls). Fingerprint detection relies on several levels of detail, each offering varying degrees of accuracy depending on the required security level. Fig 1.9 outlines these levels: Level 1 involves general ridge patterns, such as loops, whorls, and arches, which

are used for basic identification. Level 2 focuses on minutiae points, including ridge endings, bifurcations, and dots, providing more precise matching for mid-level security applications, such as personal identification in secure environments. Level 3, the highest security level, includes detailed ridge structures, skin texture, and microscopic features like sweat pores, offering the most individualized fingerprint profile for high-accuracy identification. This progression of detail enhances the reliability and precision of fingerprint recognition, ensuring its applicability in a wide range of security contexts.

1.8.2.2 *Methods of Latent Fingerprint Detection*

Various techniques are employed to detect latent fingerprints, including dusting with fine powder, chemical treatments, and the use of alternate light sources. The choice of method depends on the surface, environmental factors, and the quality of the print. Each technique is specifically designed to improve the visibility and clarity of fingerprints for forensic examination. These methods, broadly classified into chemical and physical approaches, are used to effectively visualize latent fingerprints, which are then digitized and archived through automated systems for future reference.

1.8.2.2.(i) Chemical Approaches

The chemical approach to visualizing latent fingerprints (LFPs) involves the chemical reagents that react with substances left in the print, such as amino acids, oils, or salts. Common chemicals include ninhydrin, which reacts with amino acids to produce a coloured print (Purple-blue Colour), and silver nitrate, which reacts with chloride to reveal fingerprints. The advantage of this method is its effectiveness on porous surfaces like wood, cardboard, paper, where physical techniques may not work. However, the disadvantage is that chemical reagents can be destructive or damaging to the surface, potentially compromising other evidence.

Additionally, some methods may require careful handling due to toxicity or sensitivity to environmental conditions.

1.8.2.2.(ii) Physical Approaches

Powder dusting is a commonly used physical technique for visualizing latent fingerprints (LFPs). It involves applying a fine powder to a surface, where it adheres to the oils and residues left by the fingerprint, making the print visible. The powder is typically applied using a brush or magnetic applicator, with the colour chosen based on the surface colour, type and texture (e.g., black, white, magnetic, or gray powder). Once the print is visualized, it can be photographed or lifted using adhesive tape. This method is quick, non-invasive, and effective for non-porous surfaces like glass, metal, and plastic. However, it is less effective on porous surfaces like paper and may not reveal high-detail prints on textured or contaminated surfaces. Additionally, dusting can leave residue or damage delicate surfaces. In some cases, magnetic powdering provides a gentler alternative for porous surfaces, while methods like ninhydrin and Small Particle Reagent (SPR) are more suitable for porous or greasy surfaces.

1.8.2.3 *Application of luminescent materials*

Phosphor materials offer a promising alternative to traditional dusting techniques for LFP detection, providing several notable advantages. Both traditional and lanthanide (Ln)-doped phosphors require an excitation source for illumination, followed by similar procedure for detecting LFPs as in dusting approach. As shown in Fig 1.10, the general procedure for revealing latent fingerprints with luminescent powders is illustrated. The process begins with the deposition of the fingerprint (Fig. 1.10a), where a finger is lightly pressed onto a surface, leaving behind a natural, unintentional print. In the next step (Fig. 1.10b), luminescent powder

is applied to the fingerprint, and excess powder is gently brushed away, exposing the ridge details of the print. The fingerprint is then transferred onto transparent tape (Fig. 1.10c), which helps preserve finer details for further analysis. Finally, UV light is used to excite the luminescent powder on the surface, causing the fingerprint to glow (Fig. 1.10d), and a high-resolution camera captures the image for comparison with existing databases.

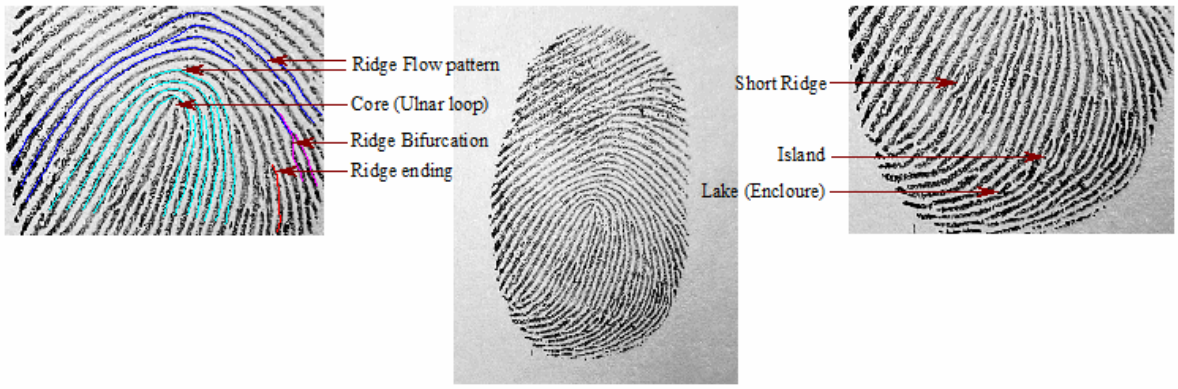

Figure 1.9 Fingerprint features (a) Level 1, (b) Level 2, (c) Level 3 [47].

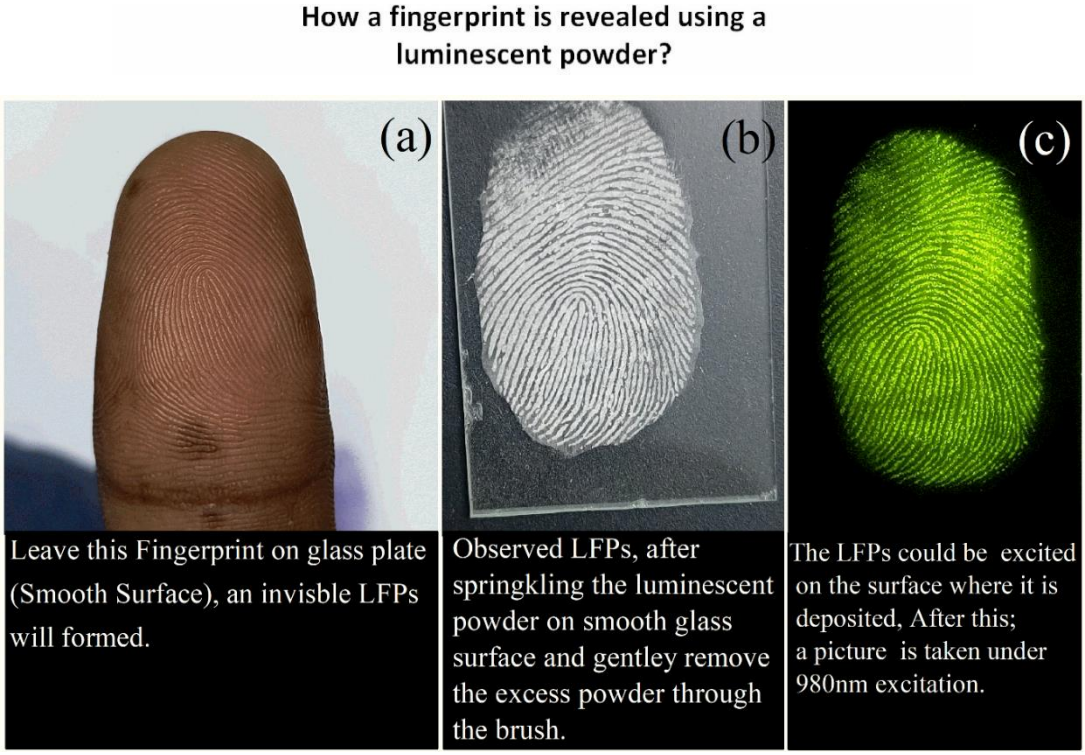

Figure 1.10 General procedure to reveal fingerprints on any surface [48].

This thesis examines Ln^{3+}-activated phosphor materials, especially UCNPs having dual excitation behaviour, which require a specific excitation source to activate the phosphor sample. Traditional phosphors have broad emission spectra, which restrict their performance, while Ln-doped phosphors provide narrow, tunable spectra, high quantum efficiency, and persistent fluorescence, improving the sensitivity, accuracy, and contrast in latent fingerprint detection under UV or near-infrared light. This results in superior clarity and effectiveness, especially on non-porous surfaces like glass, metal, or plastic, where traditional dusting methods may be less successful. Lanthanide phosphors can reveal fingerprints with high detail, even in low-light conditions, making them ideal for LFPs detection. The key advantage of using lanthanide-activated phosphors is their non-destructive nature. Unlike chemical methods, which may damage surfaces or other evidence, phosphors simply provide a visual marker, allowing for the preservation of the original surface. Additionally, these materials can be tailored for specific wavelengths of light, offering versatility for a wide range of surfaces and environmental conditions. Despite being more expensive and requiring specialized equipment like UV or laser light sources and detection cameras, lanthanide phosphors offer enhanced performance and versatility in forensic fingerprint analysis. Their fine nanoparticle size also poses handling and contamination challenges, but their superior capabilities make them a valuable alternative to traditional methods.

In my PhD research, I investigated the potential use of $Ho^{3+}/Tm^{3+}/Yb^{3+}$-doped $CaMoO_4$ phosphor materials for latent fingerprint detection. These materials exhibit distinctive luminescent properties when excited by near-infrared (NIR) light, offering enhanced fingerprint visualization with high contrast and clear ridge detail. This innovative approach

aligns with recent advancements in forensic science, where high-resolution imaging and luminescent techniques are increasingly utilized for reliable fingerprint identification.

1.9 Conclusion

This introductory chapter has provided the framework for the research presented in this thesis by delving into the essential ideas and history of luminous materials and their applications. Starting with a historical overview and theoretical foundation of lanthanides, I have explored the principles of luminescence, encompassing both downconversion and upconversion mechanisms. Additionally, I have examined the role of inorganic phosphor hosts, with particular emphasis on $CaMoO_4$ as a stable and effective matrix for lanthanide doping. The unique properties of lanthanides, including Er, Ho, Tm, and Yb, have been analyzed in terms of their luminescent characteristics and their potential for dual-mode emission applications.

The chapter also examined the application of $CaMoO_4$-based phosphors in temperature sensing and latent fingerprint detection. In the context of temperature sensing, both thermally coupled and non-thermally coupled energy levels were discussed, highlighting the advantages of Er ions for thermally coupled applications and Ho and Tm ions for non-thermally coupled applications. The principles of contactless optical thermometry and its applicability in extreme or non-intrusive environments were highlighted, showcasing the potential for precise, non-invasive temperature measurements across a broad range of conditions. Furthermore, the role of Ho/Tm/Yb-doped $CaMoO_4$ phosphors in enhancing latent fingerprint detection was discussed as a significant application in forensic science. The unique luminescent properties of these doped materials under near-infrared (NIR) excitation were identified as advantageous for high-contrast imaging of fingerprints, thus enhancing reliability and detail in forensic

analysis. By providing a solid theoretical and application-focused foundation, this chapter has set the stage for the research directions explored in the following chapters, where experimental studies and practical applications of these phosphor materials in temperature sensing and forensic detection are examined in detail. This introduction underscores the interdisciplinary relevance of lanthanide-doped $CaMoO_4$ materials, setting the stage for the contributions to material science, optics, and forensic applications that follow.

1.10 Organization of the thesis

This thesis is structured into six chapters. The first two chapters cover the fundamental aspects of luminescence and core properties of $CaMoO_4$ phosphors, along with the synthesis methods used for material preparation and the experimental techniques employed for sample analysis. The subsequent chapters focus on the analysis of material properties with lanthanide doping and explored their potential applications in contactless optical thermometry and latent fingerprint detection. The objectives of each chapter are summarized as follows:

Chapter 1 introduces the foundation of the research, starting with a historical perspective on luminescence and the evolution of phosphor materials, followed by a discussion on the unique role of rare earth elements (lanthanides) in optical applications. The chapter examines the distinct spectroscopic properties of lanthanides, covering key concepts such as selection rules, energy level splitting, and primary emission mechanisms. Detailed discussions of downconversion processes, including downshifting and quantum cutting, and upconversion mechanisms such as ground state absorption, excited state absorption, energy transfer upconversion, and photon avalanche provide insight into the fundamental light-emission processes central to this research. Additionally, the properties of the $CaMoO_4$ host material,

including its crystal structure, stability, and optical characteristics, are discussed with an emphasis on its suitability for lanthanide doping. Applications in temperature sensing and latent fingerprint detection are introduced, setting the stage for the subsequent experimental studies. The chapter concludes with an articulation of the motivation behind the thesis.

Chapter 2 presents an in-depth examination of the synthesis methods used to prepare lanthanide-doped $CaMoO_4$ phosphors, with particular emphasis on the hydrothermal process, valued for its efficiency in producing high-quality samples. This chapter provides a thorough account of the materials, synthesis techniques, and post-synthesis treatment methods employed in phosphor preparation. It also outlines the various characterization techniques integral to the thesis, including Powder X-ray Diffraction (XRD) for structural analysis, Scanning Electron Microscopy (SEM) and Transmission Electron Microscopy (TEM) for morphological examination, as well as Fourier Transform Infrared (FTIR) and Raman spectroscopy for structural verification. Optical properties are characterized through Ultraviolet-Visible-Near Infrared (UV-Vis-NIR) absorption spectroscopy, upconversion measurements, photoluminescence, and decay analysis. Furthermore, methodologies for temperature sensing measurements and latent fingerprint visualization are discussed, forming the basis for the analyses presented in the subsequent chapters.

Chapter 3 investigates the temperature sensing capabilities of $Ca_{0.79}Er_{0.01}Yb_{0.2}MoO_4$ phosphors, focusing on a comparative analysis between bulk (SCEY) and nanoparticle (CCEY) forms synthesized via solid-state and solution combustion methods, respectively. Through a detailed assessment of phase structure, phonon frequency, and both upconversion and downshifting properties, this chapter explores how particle size and morphology influence optical temperature sensitivity. Temperature sensitivity measurements between 305

K and 573 K reveal that the nanoparticle-based CCEY phosphor exhibits significantly enhanced sensitivity, with maximum relative and absolute sensitivities of 0.0094 K^{-1} and 0.0170 K^{-1}, respectively. These findings underscore the advantages of nanoscale $Ca_{0.79}Er_{0.01}Yb_{0.2}MoO_4$ in improving temperature sensing performance, providing valuable insights for future sensor development.

Chapter 4 builds upon the findings of Chapter 3 by investigating the influence of Bi^{3+} co-doping on the temperature sensing properties of $Ca_{0.79-x}Bi_xEr_{0.01}Yb_{0.2}MoO_4$ phosphors. Here, Bi^{3+} is introduced as a tertiary dopant to induce local symmetry distortions around Er^{3+} ions, enhancing upconversion (UC) emission without disrupting the material's overall tetragonal structure. This co-doping introduces asymmetry around Er^{3+} ions, which boosts UC emission and temperature sensitivity by reducing non-radiative decay pathways. XRD analysis demonstrates that Bi^{3+} co-doping decreases dislocation density and micro-strain within the crystal lattice, contributing further to UC enhancement. The results show a 25-fold increase in UC emission with Bi^{3+} co-doping and a corresponding improvement in temperature sensitivity, with relative sensitivities reaching 0.0068 K^{-1} at 300 K. This chapter highlights the role of Bi^{3+} in optimizing crystal structure and emission properties, paving the way for high-performance materials in optical temperature sensing.

Chapter 5 explores $CaMoO_4$: $Ho^{3+}/Tm^{3+}/Yb^{3+}$ phosphors for dual applications, namely non-thermally coupled levels (NTCLs)-based temperature sensing and latent fingerprint (LFP) visualization. By utilizing the distinct emission properties of Ho^{3+} and Tm^{3+} ions, temperature sensing is achieved through fluorescence intensity ratio (FIR) fitting using a Boltzmann sigmoidal function, yielding high sensitivity of 69.86×10^{-2} K^{-1} at 500 K. In parallel, the phosphor's luminescent emissions under near-infrared (NIR) excitation are

leveraged for LFP visualization through the powder dusting method, providing high-contrast imaging suitable for forensic analysis. This chapter underscores the multifunctionality of $Ho^{3+}/Tm^{3+}/Yb^{3+}$-doped $CaMoO_4$ phosphors in precise optical temperature sensing and forensic applications, demonstrating their potential in advanced sensing technologies.

Chapter 6 consolidates the primary findings of the thesis, demonstrating the effectiveness of lanthanide-doped $CaMoO_4$ phosphors for advanced optical temperature sensing and latent fingerprint detection. Through a systematic investigation of host structure, dopant selection, and synthesis methodologies, this research highlights the adaptability of $CaMoO_4$ as a robust matrix for functional lanthanide doping. The chapter concludes with recommendations for future research, suggesting further optimization of material properties and exploring broader applications in cutting-edge optical technologies.